

22 Introduction

23 Ethylene is an important building block in the modern chemical industry for the production of
24 polyethylene and many other industrial chemical compounds. The production of ethylene
25 without immediate hydrogenation to the less valuable product, ethane, remains a selectivity
26 challenge for several chemical processes. The most studied example of such processes is the
27 selective hydrogenation of acetylene to ethylene ($C_2H_2 + H_2 \rightarrow C_2H_4$). Industrially, catalytic
28 hydrogenation is the preferred method for converting acetylene impurities in cracking product
29 streams back to ethylene [1]. Pd-based catalysts are the most commonly used for this process [2].
30 Pure Pd typically over-hydrogenates acetylene to the undesirable product, ethane [3,4]. Alloying
31 Pd with a second metal effectively improves its selectivity towards ethylene. Pd-Ag is one of the
32 most widely used bimetallic alloy systems for acetylene hydrogenation [5–9]. Han et al.
33 demonstrated using TiO_2 -supported catalysts that when the Ag to Pd ratio reached 1:1 or above,
34 the bimetallic catalyst became highly selective towards ethylene formation (>80%) [5]. Other
35 promoter elements have also been studied, including Au [3,10,11], Cu [12,13], Ga [14,15], and
36 Zn [16,17].

37 Another example of a catalytic process involving the selectivity issue between ethylene and
38 ethane is the hydrodechlorination of 1,2-dichloroethane (1,2-DCA). This process is a promising
39 treatment method for industrial 1,2-DCA wastes [18]. The hydrodechlorination of 1,2-DCA can
40 proceed through either the ethylene path ($C_2H_4Cl_2 + H_2 \rightarrow C_2H_4 + 2HCl$) or the ethane path
41 ($C_2H_4Cl_2 + 2H_2 \rightarrow C_2H_6 + 2HCl$). A series of transition metal catalysts have been experimentally
42 tested for this chemistry. Monometallic Group VIII metals such as Pt [19,20] and Pd [21–23] are
43 active dechlorination catalysts, but they also hydrogenate ethylene and produce mostly ethane.
44 On the other hand, Cu is highly selective towards ethylene formation despite its low
45 dechlorination activity [19,24]. Bimetallic alloys, such as Pt-Cu [19,25–29], Pd-Ag [21,30–36],
46 Pd-Cu [24,33], Pt-Ag [37], and Pt-Sn [20,38] have been shown as the best catalysts for 1,2-DCA
47 hydrodechlorination in terms of both dechlorination activity and ethylene selectivity.
48 Vadlamannati et al. showed that a Cu to Pt atomic ratio of 3:1 or above was required for an
49 ethylene-selective Pt-Cu bimetallic catalyst [19]. Lambert and coworkers demonstrated that for a
50 Pd-Ag or Pd-Cu hydrodechlorination catalyst to be selective towards ethylene formation, the Pd
51 composition should be 33% or less [33].

52 Despite the availability of a large number of experimental studies, mechanistic insights into the
53 origin of ethylene selectivity are still lacking, which hinders the rational catalyst design and
54 improvement. In the literature, a few density functional theory (DFT) studies have been found
55 for the selective hydrogenation of acetylene [39–45]. Most of these studies point to the
56 competition between ethylene desorption and its hydrogenation as the key factor that determines
57 catalyst selectivity. Liu demonstrated in the study of Pd-doped Ag nanoclusters that the surface
58 ethylene formed from hydrogenation of acetylene can be further hydrogenated to ethane if
59 contiguous Pd sites were present [42]. Zhang et al. performed detailed reaction kinetics analyses
60 for acetylene hydrogenation on several Pd-doped Cu/CuO_x surfaces [45]. They showed that
61 ethylene selectivity can be correlated with the Gibbs free energy of ethylene adsorption and its
62 hydrogenation Gibbs free energy barrier. These DFT studies, however, focus on the detailed
63 reaction mechanisms on specific catalytic surfaces. Performing comprehensive DFT analyses for
64 a large number of candidate catalysts is time-consuming and thus not efficient for catalyst
65 screening purposes. Studt et al. performed a DFT-based catalyst screening study for the selective
66 hydrogenation of acetylene [46], where they used the heats of adsorption of ethylene and
67 acetylene as the selectivity and activity descriptors, respectively. They further correlated both
68 parameters with the heat of adsorption of a methyl group through scaling relations, which
69 allowed them to investigate a large group of catalyst candidates based on a single
70 thermochemical parameter. Their catalyst screening scheme, however, is potentially an
71 oversimplification of the reaction system, since no reaction kinetics parameters was involved.
72 For the selective dehydrogenation of ethane to ethylene, Hook and Celik proposed a model to
73 predict catalyst selectivity using the energy difference between the ethylene dehydrogenation
74 barrier and its desorption energy [47]. Their study focused on a specific set of Pt-based surface
75 alloys. Also, temperature and entropy effects were not accounted in their model.

76 Here, we seek to provide a fundamentals-based selection scheme for
77 hydrogenation/hydrodechlorination catalysts based on their ethylene product selectivity. We
78 propose a descriptor-based model where the Gibbs free energy difference between the ethylene
79 hydrogenation barrier and the ethylene desorption energy is defined as a descriptor for ethylene
80 selectivity. Our descriptor model explicitly takes into account the reaction kinetics; moreover,
81 the use of Gibbs free energy accounts for entropic effects which may become significant at
82 elevated reaction temperatures. We present the DFT-derived ethylene selectivity descriptor

83 values for a series of monometallic and bimetallic alloys surfaces. Our method allows for
84 efficient screening of candidate surfaces with reasonable accuracy for the design of highly
85 selective hydrogenation/hydrodechlorination catalysts. In addition, our approach can be easily
86 generalized and applied to other reaction systems which involve competition between the
87 desorption and reaction of an intermediate product.

88 **Methods**

89 All the DFT calculations were performed using the Vienna *Ab-initio* Simulation Package (VASP)
90 [48,49], a plane wave total energy code. The electron-ion interactions were described by the
91 projector augmented-wave (PAW) potentials [50,51], and the exchange-correlation functional
92 was described using the generalized gradient approximation (GGA-PBE) [52]. The electronic
93 wave functions were expanded using plane waves with an energy cutoff of 400 eV. The
94 dispersion interactions were accounted for by adding to the conventional Kohn-Sham DFT
95 energy a correction term evaluated using the Tkatchenko-Scheffler method with self-consistent
96 screening (TS+SCS) [53].

97 All the metal surfaces were modeled by three-atomic-layer slabs periodically repeated in a
98 supercell geometry. Each slab consisted of a (4 × 4) unit cell, which corresponds to a surface
99 coverage of 1/16 ML. Adsorption was allowed on only one side of the two exposed surfaces of
100 each slab, and the electrostatic potential was adjusted accordingly [54,55]. The topmost layer and
101 all the adsorbate atoms were fully relaxed; the bottom two layers of each slab were fixed at their
102 truncated lattice position. In the vertical direction along the surface norm, any two successive
103 slabs were separated by at least 12 Å of vacuum. The first Brillouin zone was sampled with a (4
104 × 4 × 1) Monkhorst-Pack k-point mesh [56]. Convergence of the total energy with respect to the
105 k-point set and energy cutoff was confirmed within 0.01 eV. A systematic error of 0.09–0.12 eV
106 was observed when we increased the slab thickness from three to four layers (with the bottom
107 two fixed), while the relative order of the energies remains unchanged (Table S1). Therefore, the
108 three-layer surface model serves the purpose of ranking different surfaces with reasonable
109 accuracy. Since the aim of our study is to provide a model for catalyst screening, we performed
110 all the calculations on the three-layer slabs as a compromise for the computational cost. This
111 allows for the sampling of a wide range of catalyst candidates within a short period of time. Our
112 calculated lattice constant values of all the metals and metal alloys involved in this work are

113 summarized in Table S2; in general, the calculated lattice constant values are in good agreement
114 with the experimental ones.

115 The binding energies of individual surface adsorbates were defined with respect to their gas-
116 phase energy using Equation (1):

$$117 \quad BE = E_{\text{tot}} - E_{\text{slab}} - E_{\text{gas}} \quad (1)$$

118 where BE stands for the binding energy of the adsorbate, E_{tot} for the total energy of the adsorbed
119 species and the slab, E_{slab} for the total energy of the clean slab, and E_{gas} for the total energy of the
120 adsorbate in the gas phase.

121 The transition states and activation energy barriers were identified using the climbing image
122 nudged elastic band (CI-NEB) method [57] with seven interpolated images in addition to the
123 initial and final states. The structures were relaxed until the maximum force on all images was
124 smaller than 0.1 eV/\AA . The transition states were confirmed by vibrational frequency analyses
125 [58] yielding a single imaginary frequency along the reaction coordinate. Entropies and heat
126 capacities of adsorbates and transition states were determined from the DFT-calculated
127 vibrational frequencies; detailed procedures were described in previous publications [59,60].

128 **Results and Discussion**

129 In this section, we first explain the definition of our ethylene selectivity descriptor. We then
130 present the calculated descriptor values on a series of monometallic and selected bimetallic alloy
131 surfaces and briefly explore the relationship between the kinetic and thermochemical parameters
132 in our model. In the end, we discuss implications of our results as well as potential applications
133 of this descriptor model.

134 To define the ethylene selectivity descriptor, we consider two possible reaction events when
135 ethylene is formed on the surface along with an adsorbed hydrogen atom ($\text{CH}_2\text{CH}_2^* + \text{H}^*$; *
136 denotes an adsorbed species or adsorption site): (1) desorption of both surface species to form
137 gas-phase ethylene and hydrogen ($\text{CH}_2\text{CH}_2(\text{g}) + \text{H}_2(\text{g})$), and (2) combination of both species to
138 form CH_3CH_2^* (ethylene hydrogenation: $\text{CH}_2\text{CH}_2^* + \text{H}^* \rightarrow \text{CH}_3\text{CH}_2^* + *$) through a transition
139 state ($[\text{CH}_2\text{CH}_2+\text{H}]^*_{\text{TS}}$), which would ultimately lead to the formation of ethane, through a

140 subsequent hydrogenation step. The idea is illustrated graphically by the Gibbs free energy
 141 surface shown in Figure 1. The desorption Gibbs free energy (ΔG_{des}) and hydrogenation Gibbs
 142 free energy barrier (ΔG_{TS}) are defined by Equations (2) and (3), respectively:

$$143 \quad \Delta G_{des} = G_{\text{CH}_2\text{CH}_2(\text{g})} + \frac{1}{2}G_{\text{H}_2(\text{g})} - (G_{\text{CH}_2\text{CH}_2^*} + G_{\text{H}^*}) \quad (2)$$

$$144 \quad \Delta G_{TS} = G_{[\text{CH}_2\text{CH}_2+\text{H}]^*_{TS}} - (G_{\text{CH}_2\text{CH}_2^*} + G_{\text{H}^*}) \quad (3)$$

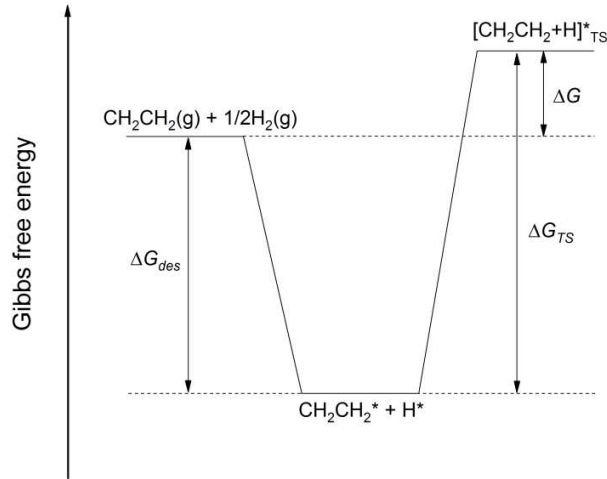
145 The ratio between the ethylene selectivity ($s_{ethylene}$) and ethane selectivity (s_{ethane}) is governed by
 146 the difference between the desorption and hydrogenation barriers as indicated in Equation (4),
 147 where k_B and T denote Boltzmann's constant and temperature, respectively:

$$148 \quad \frac{s_{ethylene}}{s_{ethane}} \propto \frac{e^{-\Delta G_{des}/k_B T}}{e^{-\Delta G_{TS}/k_B T}} = e^{(\Delta G_{TS} - \Delta G_{des})/k_B T} \quad (4)$$

149 Therefore, the ethylene selectivity descriptor (ΔG) can be defined using Equation (5):

$$150 \quad \Delta G = \Delta G_{TS} - \Delta G_{des} \quad (5)$$

151 where a larger ΔG value indicates higher selectivity towards ethylene formation.



152
 153 **Figure 1:** Graphic illustration of the definition of the ethylene selectivity descriptor (ΔG).

154 Using this descriptor model, we conducted a theoretical investigation of the ethylene/ethane
 155 selectivity over the (111) facets of three pure metals (Pt, Pd and Cu), nine Pt-based bimetallic
 156 alloys (Pt₃Cu₁, Pt₁Cu₁, Pt₁Cu₃, Pt₃Ag₁, Pt₁Ag₁, Pt₁Ag₃, Pt₃Au₁, Pt₁Au₁, and Pt₁Au₃), and nine Pd-

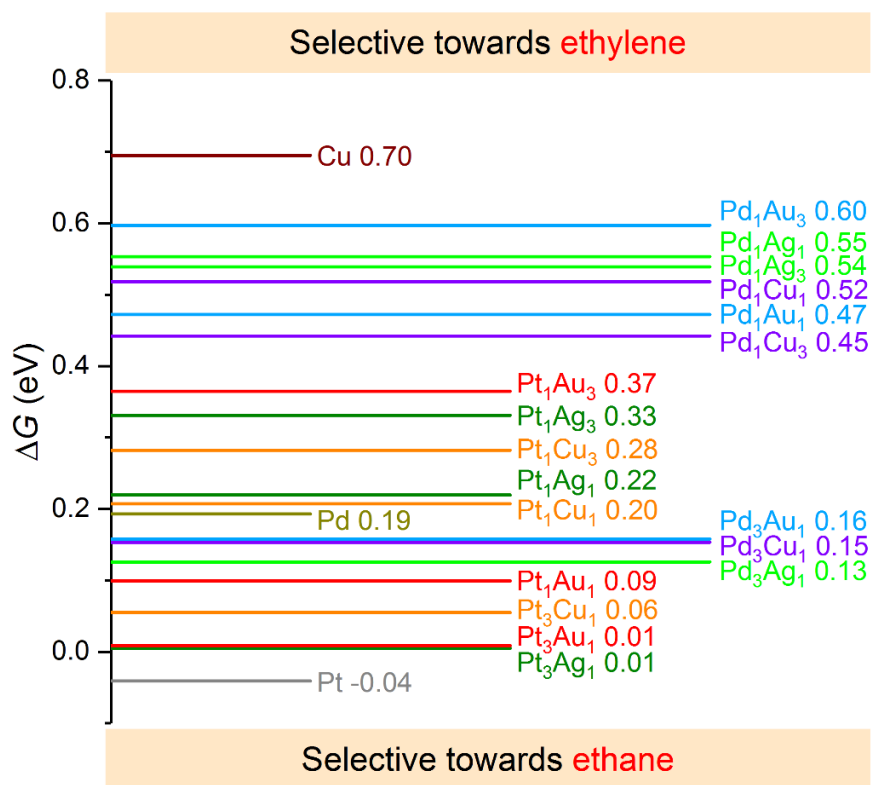
157 based bimetallic alloys (Pd₃Cu₁, Pd₁Cu₁, Pd₁Cu₃, Pd₃Ag₁, Pd₁Ag₁, Pd₁Ag₃, Pd₃Au₁, Pd₁Au₁, and
158 Pd₁Au₃). DFT calculations were performed to obtain the surface energetics and the results are
159 summarized in the Supplementary Information: the calculated binding energies and preferred
160 adsorption sites for all the surface species (H*, CH₂CH₂* and CH₃CH₂*) are listed in Table S3;
161 the optimized binding structures of the surface species and the transition states of ethylene
162 hydrogenation are shown in Figure S1; the calculated temperature-dependent thermochemistry
163 parameters of all the surface species and transition states are summarized in Table S4. We then
164 evaluated the ethylene selectivity descriptor values on the monometallic and bimetallic alloys
165 surfaces at an elevated temperature of 473 K (relevant under hydrodechlorination and
166 hydrogenation conditions) using the DFT-derived parameters. The results are summarized in
167 Figure 2 and Table S5. All the descriptor values are presented in electron-volt (eV, 1 eV = 96.5
168 kJ/mol) throughout this work; at 473 K, a difference of approximately 0.09 eV in energy is
169 equivalent to a one-order-of-magnitude difference in the selectivity ratio given the Arrhenius
170 relationship.

171 Among the monometallic surfaces, we obtained low ΔG values (thus high ethane selectivity) on
172 both of the Group VIII metal surfaces, Pt(111) (-0.04 eV) and Pd(111) (0.19 eV). Indeed, Pt and
173 Pd have been shown experimentally as active hydrogenation catalysts and selective towards
174 ethane [19–23]. On the other hand, the descriptor value is 0.70 eV on Cu(111), which is the
175 highest among all the surfaces involved in this study. This is in accord with the experimental
176 findings that Cu can be highly selective towards ethylene formation in the 1,2-DCA
177 hydrodechlorination reaction albeit its low activity [19,24,33]. The large ΔG value on Cu(111) is
178 mostly due to the weak binding of ethylene (BE = -0.63 eV), which leads to a negative
179 desorption Gibbs free energy of -0.12 eV at 473 K. Although the Gibbs free energy barrier of
180 hydrogenation on Cu(111) (0.58 eV) is also lower than those on Pt(111) (0.98 eV) and Pd(111)
181 (0.88 eV), the combined effect still yields a high ΔG value on Cu(111), which indicates that the
182 desorption of ethylene is highly preferred.

183 We now discuss the results on the bimetallic alloy surfaces. When Pt or Pd is alloyed with a
184 Group IB metal (Cu, Ag, or Au), the ethylene selectivity descriptor can be significantly altered
185 depending on the composition, which suggests that by increasing the amount of Cu, Ag, or Au in
186 Pt or Pd alloy catalysts, the ethylene selectivity can be modified. We plotted the ΔG values

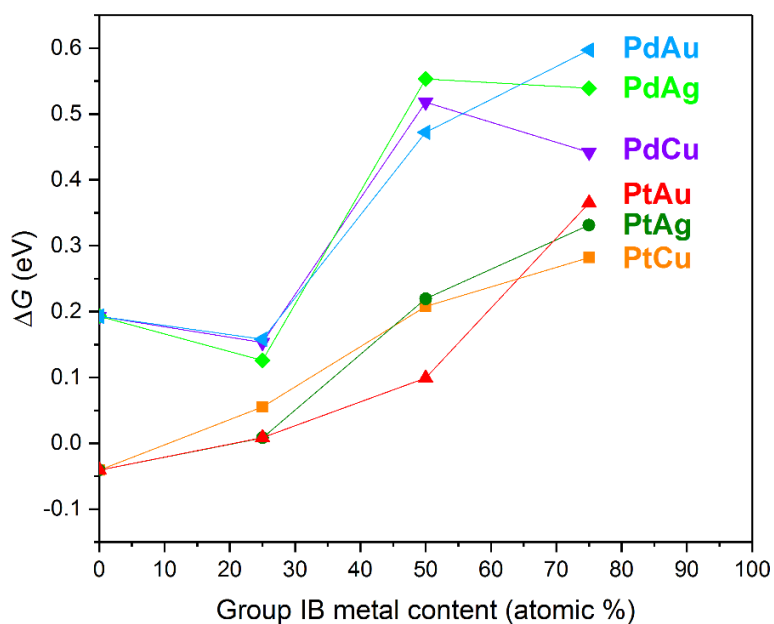
187 against the content of the Group IB (Cu, Ag, or Au) metals, as shown in Figure 3. On the Pt-
188 based alloy surfaces (orange, dark green, and red lines), we observed a general trend that ΔG
189 gradually increases with the amount of Cu, Ag or Au. The strength of the modifying effect on the
190 ethylene selectivity of Pt alloy catalysts slightly differs among the three Group IB metals at
191 different compositions. At a 1:1 Pt to Group IB metal ratio, Ag has the strongest modifying
192 effect ($\Delta G = 0.22$ eV) while Au has the weakest one ($\Delta G = 0.09$ eV); at 1:3 Pt to Group IB metal
193 ratio, however, Pt₁Au₃ becomes the surface with the largest ΔG value (0.37 eV).

194 On the Pd-based alloy surfaces (purple, light green and blue lines), a different trend was
195 observed: the descriptor value no longer increases smoothly with the Group IB metal content.
196 Interestingly, the ΔG values evaluated on all three Pd₃B₁(111) surfaces (B = Cu, Ag, or Au) are
197 lower than that on Pd(111); i.e., the addition of 25% of Group IB metal has an adverse effect on
198 the ethylene selectivity of Pd catalysts. As shown in Figure S1, ethylene prefers to adsorb and
199 react over the Pd sites on Pd₃B₁(111); the adsorption and transition state geometries resemble
200 those on the monometallic Pd(111) surface. Therefore, at 25% composition, the Group IB metal
201 only plays an indirect role of modifying surface reactivity by altering (1) the lattice size of the
202 alloy and (2) the electronic structure of the surface atoms. The different trends observed on
203 Pt₃B₁(111) and Pd₃B₁(111) surfaces reflect the distinct modifying effects of Group IB metals to
204 Pt and Pd catalysts. When the composition of Cu, Ag, or Au increases from 25% to 50% and
205 above in the Pd alloys, ΔG rises sharply. Similar to the Pt-base alloys, though, Ag has the
206 strongest modifying effect on ethylene selectivity at 50% composition (0.55 eV), while Au has
207 the strongest effect at 75% composition (0.60 eV). Compared with Pt-based alloys, Pd alloys are
208 generally associated with larger ΔG values, which indicates that Pd-based bimetallics might be
209 more promising ethylene-producing catalysts than their Pt-based counterparts.



210

211 **Figure 2:** Ethylene selectivity descriptor (ΔG) values of metals and metal alloys at 473 K. All values
 212 were evaluated based on DFT results on clean (111) facets.



213

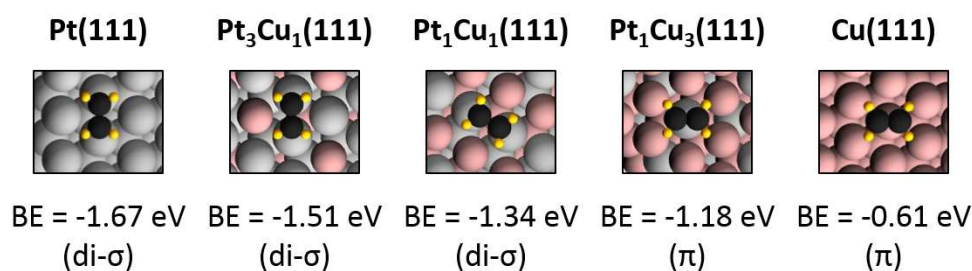
214 **Figure 3:** Ethylene selectivity descriptor (ΔG) plotted as a function of atomic percentage content of
 215 Group IB metal (Cu, Ag or Au) in the bulk alloy. Lines are added to guide the eye.

216 Based on the ΔG values presented in Figure 2, Pd₁Au₃, Pd₁Ag₁, and Pd₁Ag₃ are predicted to be
217 the three most selective alloy surfaces towards ethylene production. Experiments have indeed
218 shown that Pd-Ag and Pd-Au bimetallic catalysts possess superior ethylene selectivity in
219 acetylene hydrogenation. In particular, Han et al. reported a TiO₂-supported Pd-Ag catalyst with
220 an approximately 1:1 bulk atomic ratio which produced ~80% ethylene [5]. Ma et al. synthesized
221 Pd-Au nanoparticles supported on MgAl mixed metal oxides with a flower-like nanostructure;
222 the catalyst yielded an ethylene selectivity of up to 70% [10]. For 1,2-DCA hydrodechlorination,
223 Lambert et al. demonstrated that their SiO₂-supported Pd-Ag catalyst with a 1:2 Pd-to-Ag bulk
224 atomic ratio could produce ethylene with over 80% selectivity [33]. We conclude that our simple
225 descriptor-based model successfully captures the elemental identity of a few of the best-
226 performing catalysts reported in the literature in terms of ethylene selectivity.

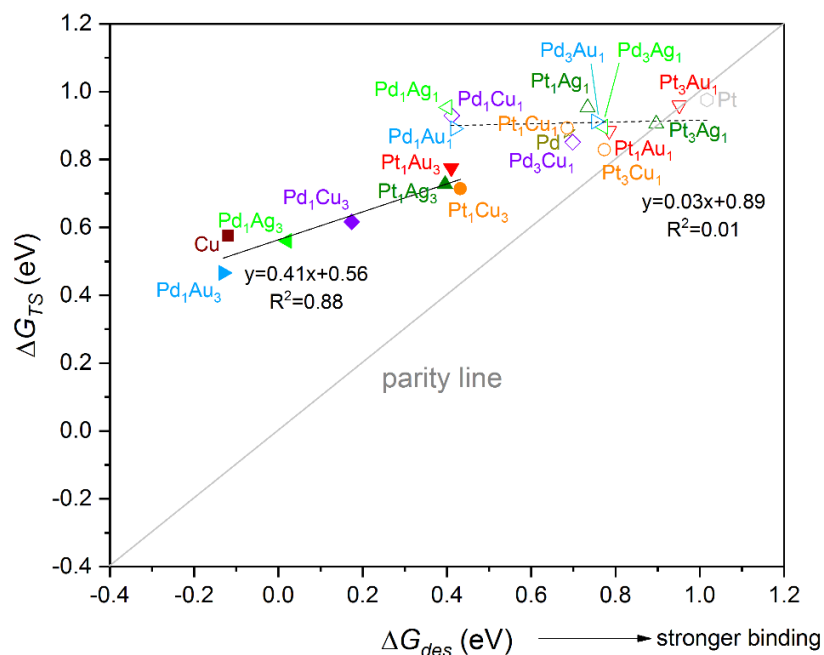
227 Brønsted–Evans–Polanyi (BEP) type of relations commonly exist in many reaction systems,
228 which empirically connect kinetic parameters with thermochemistry of reactants and/or products
229 [61–64]. Here we also explored the potential correlation between ΔG_{TS} , a kinetic parameter, and
230 ΔG_{des} , a thermochemical parameter. When the entire set of metal surfaces was taken into account,
231 we did not observe a good linear correlation between the two parameters. The poor correlation
232 can be attributed to the presence of two distinct ethylene binding structures, di- σ -bonding, and π -
233 bonding, as illustrated in Figure 4 where Pt-Cu alloys with different compositions are used as
234 examples. When a Pt ensemble of at least two atoms is present on the surface (Pt(111),
235 Pt₃Cu₁(111) and Pt₁Cu₁(111)), ethylene always prefers to bind through a di- σ -bonding structure
236 on top of two adjacent Pt atoms. When no such ensemble is present (Pt₁Cu₃(111) and Cu(111)),
237 the ethylene molecule is forced to bind through the less stable π -bonding structure. Similar trends
238 were also observed on other Pt- or Pd-based alloy surfaces.

239 The different ethylene binding structures also lead to different transition state structures of the
240 subsequent ethylene hydrogenation step. Therefore, we divided the metal and metal alloy
241 surfaces involved in this study into two groups according to the ethylene binding structures and
242 then attempted to correlate ΔG_{TS} and ΔG_{des} for each group of surfaces. The results are
243 summarized in Figure 5. On the π -bonding surfaces, we observed a good linear relationship
244 between ΔG_{TS} and ΔG_{des} with a slope of 0.41, likely due to the similar transition state structures
245 on all these metal surfaces. On the di- σ -bonding surfaces, nonetheless, the transition state

246 structures and energies vary with the surface composition. When a three-fold Pd/Pt hollow site is
 247 present on the surface, the hydrogenation reaction always occurs over these sites. However,
 248 when the composition of Pd/Pt is 50%, no such site is present, and the H atom has to approach
 249 the di-sigma ethylene species over a mixed site, in which case the transition state energy is more
 250 strongly affected by the Group IB metal. Therefore, no correlation between ΔG_{TS} and ΔG_{des} was
 251 observed on the di- σ -bonding surfaces; the ΔG_{TS} values vary in a range of 0.83–0.98 eV
 252 regardless of the ΔG_{des} values. We conclude that on the metal/metal alloy surfaces where
 253 ethylene binds through a π -bonding structure, it is possible to correlate the kinetic parameter
 254 ΔG_{TS} with ΔG_{des} , thus allowing the prediction of ΔG based on thermochemistry alone, while on
 255 the di- σ -bonding surfaces, explicit DFT calculations of the activation barriers are required to
 256 accurately predict the ΔG descriptor value.



257
 258 **Figure 4:** Illustrations of different minimum-energy binding configurations (di- σ -bonding and π -bonding)
 259 of ethylene over Pt(111), Cu(111), and Pt_xCu_y(111).



260

261 **Figure 5:** Correlation between ethylene hydrogenation Gibbs free energy barriers (ΔG_{TS}) and ethylene
 262 desorption Gibbs free energy (ΔG_{des}). The solid symbols denote surfaces that bind ethylene through π
 263 bonds. The open symbols denote surfaces that bind ethylene through di- σ bonds. The solid and dashed
 264 lines indicate the linear regression results for π -bonding and di- σ -bonding surfaces, respectively.

265 The DFT calculations involved in this work were conducted on clean surfaces, and all the alloy
 266 surfaces were kept at their bulk compositions. The accuracy of our model could thus be
 267 potentially improved by taking into account adsorbed species coverage effects and alloy
 268 component surface segregation effects. Past DFT studies have demonstrated that the presence of
 269 surface spectators can significantly impact the surface adsorption properties and reaction
 270 behaviors [65,66]. Ethylidyne (CH_3C) is a common surface-poisoning species in reaction
 271 systems involving C_2 species; in the hydrodechlorination reaction of 1,2-DCA, atomic chlorine
 272 has been proposed as another potential site-blocking species. Both species could be present on
 273 the catalytic surface under reaction conditions and thereby alter surface reaction and desorption
 274 energetics.

275 In addition, adsorption of surface species could lead to the preferential surface segregation of one
 276 of the two components in bimetallic alloys due to the different interaction strengths of adsorbates
 277 with different metals [67]. Luebke and co-workers reported in their 1,2-DCA
 278 hydrodechlorination study on Pt-Cu catalysts that the ethylene selectivity could be altered by
 279 pretreating the catalyst with HCl [25]. They attributed the effect to the surface segregation of Cu,

280 induced by chlorine adsorption, because the Cu-Cl interactions are stronger than the Pt-Cl
281 interactions. Similar segregation effects can be expected for other alloy systems. For example,
282 the Pd₁Au₃(111) surface, with the highest ΔG value among all the alloy surfaces considered in
283 this study, can be prone to Pd segregation under hydrodechlorination conditions. Since Cl binds
284 much stronger on Pd than on Au (the BEs of Cl on Pd(111) and Au(111) are -3.25 eV and -2.36
285 eV, respectively, according to our DFT calculations), Cl adsorption likely induces a Pd-rich
286 surface, which thus leads to a decrease in ethylene selectivity. The exact effects of adsorbed
287 species coverage and surface segregation of alloy components strongly depend on the actual
288 reaction conditions and are beyond the scope of this study. The *ab-initio* phase diagram has been
289 demonstrated as a powerful theoretical tool for determining relevant surface coverage and
290 composition under real reaction conditions [68–70] and can be a valuable addition to our current
291 catalyst screening scheme.

292 Despite the room for potential improvement, our analysis of the ethylene selectivity of various
293 monometallic and bimetallic alloy surfaces demonstrates the usefulness of this descriptor model
294 as a simple yet powerful tool for initial catalyst screening purposes. Instead of a detailed analysis
295 of the entire reaction network which typically involves dozens of elementary steps, our method
296 requires DFT calculations for only one elementary step per surface, thus allowing for the
297 prediction of an approximate ethylene selectivity for a large number of candidate catalytic
298 surfaces. Such a catalyst screening scheme can be easily applied to novel alloy catalytic systems
299 beyond homogeneous bulk alloys, such as near surface alloys which serve as models for core-
300 shell or “onion-structured” nanoparticles [67,71–74]. In addition, our method can be generalized
301 for other catalytic reaction systems with selectivity issues as long as there exists a competition
302 between the desorption and reaction steps of an intermediate product. For example, a selectivity
303 descriptor can be defined for the selective dehydrogenation of ethane to ethylene by comparing
304 the desorption barrier of ethylene with its dehydrogenation barrier.

305 **Conclusions**

306 In this work, we have presented a descriptor-based initial catalyst screening scheme for catalysts
307 with high selectivity towards ethylene over ethane formation, which can be potentially applied to
308 catalytic processes such as the selective hydrogenation of acetylene and the hydrodechlorination
309 of 1,2-DCA. The Gibbs free energy difference (ΔG) between the hydrogenation barrier (ΔG_{TS})

310 and desorption energy (ΔG_{des}) of adsorbed ethylene and hydrogen was defined as a descriptor for
311 the catalyst selectivity, where a larger ΔG indicates higher selectivity towards ethylene
312 desorption, as opposed to its hydrogenation. Dispersion-corrected DFT calculations (PBE-
313 TS+SCS) were performed to determine the descriptor values over the close-packed facets of Pt,
314 Pd, and Cu as well as a series of Pt_xB_y and Pd_xB_y (B = Cu, Ag or Au) bimetallic alloys with
315 different bulk compositions. Our results suggest: (1) monometallic Pt and Pd are selective
316 towards ethane formation, whereas Cu is selective towards ethylene formation; (2) the selectivity
317 descriptor value of a Pt-based alloy gradually increases with the amount of the Group IB metal
318 introduced, whereas on Pd-based alloys, the descriptor value rises sharply only when the amount
319 of Cu, Ag or Au increases from 25% to 50%; (3) among the three Group IB metals (Cu, Ag and
320 Au), Ag improves the ethylene selectivity of Pt/Pd alloy catalysts the most at 1:1 atomic ratio,
321 while Au has the strongest effect at 75% composition; (4) Pd-based alloys are superior in terms
322 of ethylene selectivity over their Pt-based counterparts; and (5) on the metal/metal alloy surfaces
323 where ethylene binds through a π -bonding structure, ΔG_{TS} correlates linearly with ΔG_{des} and thus
324 the descriptor can be estimated based on thermochemical parameters alone, while no such
325 correlation is observed on those surfaces where ethylene binds through a di- σ -bonding structure.
326 Our descriptor model offers an efficient means for the initial selection of promising catalyst
327 candidates with improved ethylene selectivity. In addition, the model can be potentially
328 generalized and applied to other reaction systems where competition between desorption and
329 reaction of key intermediates is involved.

330 **Declarations of interest:** none

331 **Acknowledgements**

332 This work is supported as part of The Dow Chemical Company University Partner Initiative with
333 UW-Madison, under Dow agreement number 235744C. We thank Dr. David Barton and Dr.
334 Thomas Gilbert at The Dow Chemical Company for their kind support for this collaboration. In
335 addition, we acknowledge Prof. James A. Dumesic at UW-Madison for his valuable advice and
336 extensive discussions. LX thanks Dr. Yunhai Bai, Dr. Anthony Plauck, Duygu Gerceker, and
337 Sean Tacey for helpful input. The computational work in this study was performed partly
338 through supercomputing resources from the following institutions: the National Energy Research
339 Scientific Computing Center (NERSC); the Center for Nanoscale Materials (CNM) at Argonne

340 National Laboratory (ANL); and the Environmental Molecular Sciences Laboratory (EMSL), a
341 national scientific user facility at Pacific Northwest National Laboratory (PNNL). EMSL is
342 sponsored by the Department of Energy's Office of Biological and Environmental Research
343 located at PNNL, whereas CNM and NERSC are supported by the U.S. Department of Energy,
344 Office of Science, under contracts DE-AC02-06CH11357 and DE-AC02-05CH11231,
345 respectively.

346 **References**

- 347 [1] A.J. McCue, J.A. Anderson, Recent advances in selective acetylene hydrogenation using
348 palladium containing catalysts, *Front. Chem. Sci. Eng.* 9 (2015) 142–153.
349 doi:10.1007/s11705-015-1516-4.
- 350 [2] W.T. McGown, C. Kemball, D.A. Whan, M.S. Scurrrell, Hydrogenation of acetylene in
351 excess ethylene on an alumina supported palladium catalyst in a static system, *J. Chem.*
352 *Soc. Faraday Trans. 1 Phys. Chem. Condens. Phases.* 73 (1977) 632.
353 doi:10.1039/f19777300632.
- 354 [3] T. V. Choudhary, C. Sivadinarayana, A.K. Datye, D. Kumar, D.W. Goodman, Acetylene
355 hydrogenation on Au-based catalysts, *Catal. Letters.* 86 (2003) 1–8.
356 doi:10.1023/A:1022694505504.
- 357 [4] A. Borodziński, G.C. Bond, Selective hydrogenation of ethyne in ethene-rich streams on
358 palladium catalysts. Part 1. Effect of changes to the catalyst during reaction, *Catal. Rev.*
359 48 (2006) 91–144. doi:10.1080/01614940500364909.
- 360 [5] Y. Han, D. Peng, Z. Xu, H. Wan, S. Zheng, D. Zhu, TiO₂ supported Pd@Ag as highly
361 selective catalysts for hydrogenation of acetylene in excess ethylene, *Chem. Commun.* 49
362 (2013) 8350. doi:10.1039/c3cc43511c.
- 363 [6] Y. Zhang, W. Diao, C.T. Williams, J.R. Monnier, Selective hydrogenation of acetylene in
364 excess ethylene using Ag- and Au-Pd/SiO₂ bimetallic catalysts prepared by electroless
365 deposition, *Appl. Catal. A Gen.* 469 (2014) 419–426. doi:10.1016/j.apcata.2013.10.024.
- 366 [7] C. Shi, R. Hoisington, B.W.L. Jang, Promotion effects of air and H₂ nonthermal plasmas
367 on TiO₂ supported Pd and Pd-Ag catalysts for selective hydrogenation of acetylene, *Ind.*
368 *Eng. Chem. Res.* 46 (2007) 4390–4395. doi:10.1021/ie0701468.
- 369 [8] J.H. Lee, S.K. Kim, I.Y. Ahn, W.J. Kim, S.H. Moon, Performance of Pd-Ag/Al₂O₃

- 370 catalysts prepared by the selective deposition of Ag onto Pd in acetylene hydrogenation,
371 Catal. Commun. 12 (2011) 1251–1254. doi:10.1016/j.catcom.2011.04.015.
- 372 [9] G.X. Pei, X.Y. Liu, A. Wang, A.F. Lee, M.A. Isaacs, L. Li, X. Pan, X. Yang, X. Wang, Z.
373 Tai, K. Wilson, T. Zhang, Ag alloyed Pd single-atom catalysts for efficient selective
374 hydrogenation of acetylene to ethylene in excess ethylene, ACS Catal. 5 (2015) 3717–
375 3725. doi:10.1021/acscatal.5b00700.
- 376 [10] C. Ma, Y. Du, J. Feng, X. Cao, J. Yang, D. Li, Fabrication of supported PdAu nanoflower
377 catalyst for partial hydrogenation of acetylene, J. Catal. 317 (2014) 263–271.
378 doi:10.1016/j.jcat.2014.06.018.
- 379 [11] A. Sárkány, O. Geszti, G. Sáfrán, Preparation of Pd_{shell}-Au_{core}/SiO₂ catalyst and catalytic
380 activity for acetylene hydrogenation, Appl. Catal. A Gen. 350 (2008) 157–163.
381 doi:10.1016/j.apcata.2008.08.012.
- 382 [12] M. Friedrich, S.A. Villaseca, L. Szentmiklósi, D. Teschner, M. Armbrüster, Order-
383 induced selectivity increase of Cu₆₀Pd₄₀ in the semi-hydrogenation of acetylene, Materials.
384 6 (2013) 2958–2977. doi:10.3390/ma6072958.
- 385 [13] S.K. Kim, J.H. Lee, I.Y. Ahn, W.J. Kim, S.H. Moon, Performance of Cu-promoted Pd
386 catalysts prepared by adding Cu using a surface redox method in acetylene hydrogenation,
387 Appl. Catal. A Gen. 401 (2011) 12–19. doi:10.1016/j.apcata.2011.04.048.
- 388 [14] J. Osswald, R. Giedigkeit, R. Jentoft, M. Armbrüster, F. Girgsdies, K. Kovnir, T. Ressler,
389 Y. Grin, R. Schlogl, Palladium–gallium intermetallic compounds for the selective
390 hydrogenation of acetylene. Part I: Preparation and structural investigation under reaction
391 conditions, J. Catal. 258 (2008) 210–218. doi:10.1016/j.jcat.2008.06.013.
- 392 [15] J. Osswald, K. Kovnir, M. Armbrüster, R. Giedigkeit, R.E. Jentoft, U. Wild, Y. Grin, R.
393 Schlögl, Palladium-gallium intermetallic compounds for the selective hydrogenation of
394 acetylene. Part II: Surface characterization and catalytic performance, J. Catal. 258 (2008)
395 219–227. doi:10.1016/j.jcat.2008.06.014.
- 396 [16] H. Zhou, X. Yang, L. Li, X. Liu, Y. Huang, X. Pan, A. Wang, J. Li, T. Zhang, PdZn
397 intermetallic nanostructure with Pd-Zn-Pd ensembles for highly active and chemoselective
398 semi-hydrogenation of acetylene, ACS Catal. 6 (2016) 1054–1061.
399 doi:10.1021/acscatal.5b01933.
- 400 [17] S. Chinayon, O. Mekasuwandumrong, P. Prasertthdam, J. Panpranot, Selective

- 401 hydrogenation of acetylene over Pd catalysts supported on nanocrystalline α -Al₂O₃ and
402 Zn-modified α -Al₂O₃, *Catal. Commun.* 9 (2008) 2297–2302.
403 doi:10.1016/j.catcom.2008.03.032.
- 404 [18] V.I. Kovalchuk, J.L. d'Itri, Catalytic chemistry of chloro- and chlorofluorocarbon
405 dehalogenation: from macroscopic observations to molecular level understanding, *Appl.*
406 *Catal. A Gen.* 271 (2004) 13–25. doi:10.1016/j.apcata.2004.02.042.
- 407 [19] L. Vadlamannati, V.I. Kovalchuk, J.L. d'Itri, Dechlorination of 1,2-dichloroethane
408 catalyzed by Pt–Cu/C: unraveling the role of each metal, *Catal. Letters.* 58 (1999) 173–
409 178. doi: 10.1023/A:1019015009078.
- 410 [20] W. Rhodes, K. Lazar, V.I. Kovalchuk, J.L. d'Itri, Hydrogen-assisted 1,2-dichloroethane
411 dechlorination catalyzed by Pt–Sn/SiO₂: Effect of the Pt/Sn atomic ratio, *J. Catal.* 211
412 (2002) 173–182. doi:10.1006/jcat.2002.3731.
- 413 [21] B. Heinrichs, J.-P. Schoebrechts, J.-P. Pirard, Palladium–silver sol–gel catalysts for
414 selective hydrodechlorination of 1,2-Dichloroethane into ethylene III. Kinetics and
415 reaction mechanism, *J. Catal.* 200 (2001) 309–320. doi:10.1006/jcat.2001.3188.
- 416 [22] S. Lambert, J.-F. Polard, J.-P. Pirard, B. Heinrichs, Improvement of metal dispersion in
417 Pd/SiO₂ cogelled xerogel catalysts for 1,2-dichloroethane hydrodechlorination, *Appl.*
418 *Catal. B Environ.* 50 (2004) 127–140. doi:10.1016/j.apcatb.2004.01.015.
- 419 [23] A. Śrębowata, W. Juszczak, Z. Kaszukur, Z. Karpiński, Hydrodechlorination of 1,2-
420 dichloroethane on active carbon supported palladium–nickel catalysts, *Catal. Today.* 124
421 (2007) 28–35. doi:10.1016/j.cattod.2007.02.010.
- 422 [24] A. Śrębowata, W. Lisowski, J.W. Sobczak, Z. Karpiński, Hydrogen-assisted
423 dechlorination of 1,2-dichloroethane on active carbon supported palladium–copper
424 catalysts, *Catal. Today.* 175 (2011) 576–584. doi:10.1016/j.cattod.2011.03.038.
- 425 [25] D.R. Luebke, L.S. Vadlamannati, V.I. Kovalchuk, J.L. d'Itri, Hydrodechlorination of 1,2-
426 dichloroethane catalyzed by Pt–Cu/C: effect of catalyst pretreatment, *Appl. Catal. B*
427 *Environ.* 35 (2002) 211–217. doi:10.1016/S0926-3373(01)00257-0.
- 428 [26] V.Y. Borovkov, D.R. Luebke, V.I. Kovalchuk, J.L. d'Itri, Hydrogen-assisted 1,2-
429 dichloroethane dechlorination catalyzed by Pt–Cu/SiO₂: Evidence for different functions
430 of Pt and Cu sites, *J. Phys. Chem. B.* 107 (2003) 5568–5574. doi:10.1021/jp0300389.
- 431 [27] L. Li, X. Wang, A. Wang, J. Shen, T. Zhang, Relationship between adsorption properties

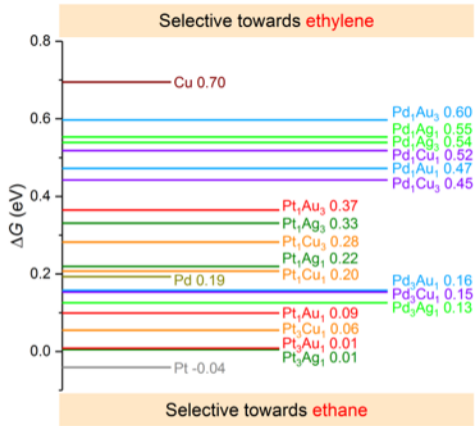
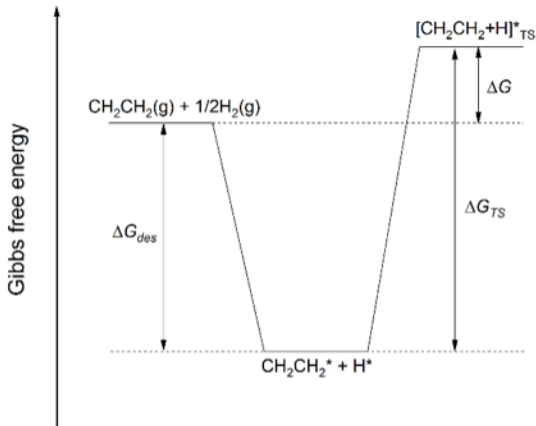
- 432 of Pt–Cu/SiO₂ catalysts and their catalytic performance for selective hydrodechlorination
433 of 1,2-dichloroethane to ethylene, *Thermochim. Acta.* 494 (2009) 99–103.
434 doi:10.1016/j.tca.2009.04.025.
- 435 [28] L.N. Akonwie, D.V. Kazachkin, D.R. Luebke, J.L. d'Itri, Effect of catalyst pre-reduction
436 temperature on the reaction of 1,2-dichloroethane and H₂ catalyzed by SiO₂-supported
437 PtCu bimetallics, *Appl. Catal. A Gen.* 415–416 (2012) 59–69.
438 doi:10.1016/j.apcata.2011.12.002.
- 439 [29] X. Wei, A.-Q. Wang, X.-F. Yang, L. Li, T. Zhang, Synthesis of Pt-Cu/SiO₂ catalysts with
440 different structures and their application in hydrodechlorination of 1,2-dichloroethane,
441 *Appl. Catal. B Environ.* 121–122 (2012) 105–114. doi:10.1016/j.apcatb.2012.03.020.
- 442 [30] B. Heinrichs, P. Delhez, J. Schoebrechts, J. Pirard, Palladium–silver sol-gel catalysts for
443 selective hydrodechlorination of 1,2-dichloroethane into ethylene I. Synthesis and
444 characterization, *J. Catal.* 172 (1997) 322–335. doi:10.1006/jcat.1997.1881.
- 445 [31] B. Heinrichs, F. Noville, J.-P. Schoebrechts, J.-P. Pirard, Palladium–silver sol-gel
446 catalysts for selective hydrodechlorination of 1,2-dichloroethane into ethylene II. Surface
447 composition of alloy particles, *J. Catal.* 192 (2000) 108–118. doi:10.1006/jcat.2000.2816.
- 448 [32] B. Heinrichs, F. Noville, J.-P. Schoebrechts, J.-P. Pirard, Palladium–silver sol-gel
449 catalysts for selective hydrodechlorination of 1,2-dichloroethane into ethylene IV.
450 Deactivation mechanism and regeneration, *J. Catal.* 220 (2003) 215–225.
451 doi:10.1016/j.jcat.2003.07.006.
- 452 [33] S. Lambert, F. Ferauche, A. Brasseur, J.-P. Pirard, B. Heinrichs, Pd–Ag/SiO₂ and Pd–
453 Cu/SiO₂ cogelled xerogel catalysts for selective hydrodechlorination of 1,2-dichloroethane
454 into ethylene, *Catal. Today.* 100 (2005) 283–289. doi:10.1016/j.cattod.2004.08.015.
- 455 [34] S.L. Pirard, J.-P. Pirard, G. Heyen, J.-P. Schoebrechts, B. Heinrichs, Experimental
456 procedure and statistical data treatment for the kinetic study of selective
457 hydrodechlorination of 1,2-dichloroethane into ethylene over a Pd-Ag sol-gel catalyst,
458 *Chem. Eng. J.* 173 (2011) 801–812. doi:10.1016/j.cej.2011.07.002.
- 459 [35] Y. Han, G. Gu, J. Sun, W. Wang, H. Wan, Z. Xu, S. Zheng, Selective hydrodechlorination
460 of 1,2-dichloroethane to ethylene over Pd-Ag/Al₂O₃ catalysts prepared by surface
461 reduction, *Appl. Surf. Sci.* 355 (2015) 183–190. doi:10.1016/j.apsusc.2015.06.164.
- 462 [36] Y. Han, J. Sun, H. Fu, X. Qu, H. Wan, Z. Xu, S. Zheng, Highly selective

- 463 hydrodechlorination of 1,2-dichloroethane to ethylene over Ag-Pd/ZrO₂ catalysts with
464 trace Pd, *Appl. Catal. A Gen.* 519 (2016) 1–6. doi:10.1016/j.apcata.2016.03.017.
- 465 [37] Y. Han, J. Zhou, W. Wang, H. Wan, Z. Xu, S. Zheng, D. Zhu, Enhanced selective
466 hydrodechlorination of 1,2-dichloroethane to ethylene on Pt–Ag/TiO₂ catalysts prepared
467 by sequential photodeposition, *Appl. Catal. B Environ.* 125 (2012) 172–179.
468 doi:10.1016/j.apcatb.2012.05.016.
- 469 [38] W. Rhodes, J. Margitfalvi, I. Borbath, K. Lazar, V.I. Kovalchuk, J.L. d'Itri, Hydrogen-
470 assisted 1,2-dichloroethane dechlorination catalyzed by Pt–Sn/SiO₂ catalysts of different
471 preparations, *J. Catal.* 230 (2005) 86–97. doi:10.1016/j.jcat.2004.11.019.
- 472 [39] D. Mei, M. Neurock, C.M. Smith, Hydrogenation of acetylene-ethylene mixtures over Pd
473 and Pd-Ag alloys: First-principles-based kinetic Monte Carlo simulations, *J. Catal.* 268
474 (2009) 181–195. doi:10.1016/j.jcat.2009.09.004.
- 475 [40] X. Xie, X. Song, W. Dong, Z. Liang, C. Fan, P. Han, Adsorption mechanism of acetylene
476 hydrogenation, *Chinese J. Chem.* 32 (2014) 631–636. doi:10.1002/cjoc.201400182.
- 477 [41] L.-D. Meng, G.-C. Wang, A DFT + U study of acetylene selective hydrogenation over
478 anatase supported Pd_aAg_b (a + b = 4) cluster, *Phys. Chem. Chem. Phys.* 16 (2014) 17541.
479 doi:10.1039/C4CP01818D.
- 480 [42] D. Liu, DFT study of selective hydrogenation of acetylene to ethylene on Pd doping Ag
481 nanoclusters, *Appl. Surf. Sci.* 386 (2016) 125–137. doi:10.1016/j.apsusc.2016.06.013.
- 482 [43] B. Yang, R. Burch, C. Hardacre, P. Hu, P. Hughes, Selective hydrogenation of acetylene
483 over Cu(211), Ag(211) and Au(211): Horiuti–Polanyi mechanism vs. non-Horiuti–Polanyi
484 mechanism, *Catal. Sci. Technol.* 7 (2017) 1508–1514. doi:10.1039/C6CY02587K.
- 485 [44] P.A. Sheth, M. Neurock, C.M. Smith, A first-principles analysis of acetylene
486 hydrogenation over Pd(111), *J. Phys. Chem. B.* 107 (2003) 2009–2017.
487 doi:10.1021/jp021342p.
- 488 [45] R. Zhang, J. Zhang, B. Zhao, L. He, A. Wang, B. Wang, Insight into the effects of Cu
489 component and the promoter on the selectivity and activity for efficient removal of
490 acetylene from ethylene on Cu-based catalyst, *J. Phys. Chem. C.* 121 (2017) 27936–27949.
491 doi: 10.1021/acs.jpcc.7b08125.
- 492 [46] F. Studt, F. Abild-Pedersen, T. Bligaard, R.Z. Sørensen, C.H. Christensen, J.K. Nørskov,
493 Identification of non-precious metal alloy catalysts for selective hydrogenation of

- acetylene., *Science*. 320 (2008) 1320–2. doi:10.1126/science.1156660.
- [47] A. Hook, F.E. Celik, Predicting selectivity for ethane dehydrogenation and coke formation pathways over model Pt-M surface alloys with ab initio and scaling method, *J. Phys. Chem. C*. 121 (2017) 17882–17892. doi:10.1021/acs.jpcc.7b03789.
- [48] G. Kresse, J. Furthmüller, Efficiency of ab-initio total energy calculations for metals and semiconductors using a plane-wave basis set, *Comput. Mater. Sci.* 6 (1996) 15–50. doi:10.1016/0927-0256(96)00008-0.
- [49] G. Kresse, J. Furthmüller, Efficient iterative schemes for ab initio total-energy calculations using a plane-wave basis set, *Phys. Rev. B. Condens. Matter*. 54 (1996) 11169–11186. doi:10.1103/PhysRevB.54.11169.
- [50] P. Blöchl, Projector augmented-wave method, *Phys. Rev. B*. 50 (1994) 17953–17979. doi:10.1103/PhysRevB.50.17953.
- [51] G. Kresse, D. Joubert, From ultrasoft pseudopotentials to the projector augmented-wave method, *Phys. Rev. B*. 59 (1999) 11–19. doi:10.1103/PhysRevB.59.1758.
- [52] J.P. Perdew, K. Burke, M. Ernzerhof, Generalized gradient approximation made simple, *Phys. Rev. Lett.* 77 (1996) 3865–3868. doi:10.1103/PhysRevLett.77.3865.
- [53] A. Tkatchenko, R.A. Distasio, R. Car, M. Scheffler, Accurate and efficient method for many-body van der Waals interactions, *Phys. Rev. Lett.* 108 (2012) 236402. doi:10.1103/PhysRevLett.108.236402.
- [54] J. Neugebauer, M. Scheffler, Adsorbate-substrate and adsorbate-adsorbate interactions of Na and K adlayers on Al(111), *Phys. Rev. B*. 46 (1992) 16067–16080. doi:10.1103/PhysRevB.46.16067.
- [55] L. Bengtsson, Dipole correction for surface supercell calculations, *Phys. Rev. B*. 59 (1999) 12301–12304. doi:10.1103/PhysRevB.59.12301.
- [56] H. Monkhorst, J. Pack, Special points for Brillouin-zone integrations, *Phys. Rev. B*. 13 (1976) 5188–5192. doi:10.1103/PhysRevB.13.5188.
- [57] G. Henkelman, H. Jónsson, Improved tangent estimate in the nudged elastic band method for finding minimum energy paths and saddle points, *J. Chem. Phys.* 113 (2000) 9978–9985. doi:10.1063/1.1323224.
- [58] J. Greeley, M. Mavrikakis, A first-principles study of surface and subsurface H on and in Ni(111): Diffusional properties and coverage-dependent behavior, *Surf. Sci.* 540 (2003)

- 525 215–229. doi:10.1016/S0039-6028(03)00790-8.
- 526 [59] A. Gokhale, S. Kandoi, J. Greeley, Molecular-level descriptions of surface chemistry in
527 kinetic models using density functional theory, *Chem. Eng. Sci.* 59 (2004) 4679–4691.
528 doi:10.1016/j.ces.2004.09.038.
- 529 [60] L.C. Grabow, M. Mavrikakis, Mechanism of methanol synthesis on Cu through CO₂ and
530 CO hydrogenation, *ACS Catal.* 1 (2011) 365–384. doi:10.1021/cs200055d.
- 531 [61] J.K. Nørskov, T. Bligaard, J. Rossmeisl, C.H. Christensen, Towards the computational
532 design of solid catalysts, *Nat. Chem.* 1 (2009) 37–46. doi:10.1038/nchem.121.
- 533 [62] P. Ferrin, D. Simonetti, S. Kandoi, E. Kunkes, J.A. Dumesic, J.K. Nørskov, M.
534 Mavrikakis, Modeling ethanol decomposition on transition metals: A combined
535 application of scaling and Brønsted-Evans-Polanyi relations, *J. Am. Chem. Soc.* 131
536 (2009) 5809–5815. doi:10.1021/ja8099322.
- 537 [63] J. Nørskov, Universality in heterogeneous catalysis, *J. Catal.* 209 (2002) 275–278.
538 doi:10.1006/jcat.2002.3615.
- 539 [64] T. Bligaard, J.K. Nørskov, S. Dahl, J. Matthiesen, C.H. Christensen, J. Sehested, The
540 Brønsted–Evans–Polanyi relation and the volcano curve in heterogeneous catalysis, *J.*
541 *Catal.* 224 (2004) 206–217. doi:10.1016/j.jcat.2004.02.034.
- 542 [65] M. Ojeda, A. Li, R. Nabar, A.U. Nilekar, M. Mavrikakis, E. Iglesia, Kinetically relevant
543 steps and H₂/D₂ isotope effects in fischer-tropsch synthesis on Fe and Co catalysts, *J. Phys.*
544 *Chem. C.* 114 (2010) 19761–19770. doi:10.1021/jp1073076.
- 545 [66] R.B. Getman, W.F. Schneider, DFT-based coverage-dependent model of Pt-catalyzed NO
546 oxidation, *ChemCatChem.* 2 (2010) 1450–1460. doi:10.1002/cctc.201000146.
- 547 [67] J. Greeley, M. Mavrikakis, Alloy catalysts designed from first principles., *Nat. Mater.* 3
548 (2004) 810–5. doi:10.1038/nmat1223.
- 549 [68] M. Bollinger, K. Jacobsen, J. Nørskov, Atomic and electronic structure of MoS₂
550 nanoparticles, *Phys. Rev. B.* 67 (2003) 85410. doi:10.1103/PhysRevB.67.085410.
- 551 [69] K. Reuter, M. Scheffler, Composition, structure, and stability of RuO₂(110) as a function
552 of oxygen pressure, *Phys. Rev. B.* 65 (2001) 35406. doi:10.1103/PhysRevB.65.035406.
- 553 [70] J.A. Herron, M. Mavrikakis, On the composition of bimetallic near-surface alloys in the
554 presence of oxygen and carbon monoxide, 2014. doi:10.1016/j.catcom.2013.10.021.
- 555 [71] F. Besenbacher, I. Chorkendorff, B.S. Clausen, B. Hammer, A.M. Molenbroek, J.K.

- 556 Nørskov, I. Stensgaard, Design of a Surface Alloy Catalyst for Steam Reforming, *Science*
557 (80-.). 279 (1998). doi:10.1126/science.279.5358.1913.
- 558 [72] P. Strasser, S. Koh, T. Anniyev, J. Greeley, K. More, C. Yu, Z. Liu, S. Kaya, D. Nordlund,
559 H. Ogasawara, M.F. Toney, A. Nilsson, Lattice-strain control of the activity in dealloyed
560 core-shell fuel cell catalysts., *Nat. Chem.* 2 (2010) 454–60. doi:10.1038/nchem.623.
- 561 [73] L. Yang, M.B. Vukmirovic, D. Su, K. Sasaki, J.A. Herron, M. Mavrikakis, L. Shijun, R.R.
562 Adzic, Tuning the catalytic activity of Ru@ Pt core-shell nanoparticles for the oxygen
563 reduction reaction by varying the shell thickness, *J. Phys. Chem. C.* 117 (2013) 1748–
564 1753. doi:10.1021/jp309990e.
- 565 [74] J.A. Herron, J. Jiao, K. Hahn, G. Peng, R.R. Adzic, M. Mavrikakis, Oxygen reduction
566 reaction on platinum-terminated “onion-structured” alloy catalysts, *Electrocatalysis.* 3
567 (2012) 192–202. doi:10.1007/s12678-012-0087-0.



ΔG – Ethylene selectivity descriptor